Int J Adv Manuf Technol (2016) 86:737–745
DOI 10.1007/s00170-015-8190-z

ORIGINAL ARTICLE

FEM-based prediction of heat partition in dry metal cutting of AISI 1045

Hendrik Puls[1] · **Fritz Klocke**[1] · **Drazen Veselovac**[1]

Received: 27 July 2015 / Accepted: 30 November 2015 / Published online: 23 December 2015

Abstract Thermal effects often limit the performance of cutting processes. The energy spent in cutting is almost completely converted into heat which partly flows to workpiece, chip, and tool during the process. Therefore, knowledge about this partition is valuable for the process, tool, and coolant system design or for the compensation of thermal deformations of the workpiece and machine tool. For this reason, a simulation model based on the finite element method was developed to analyze the heat partition in dry metal cutting. The model utilizes the coupled Eulerian-Lagrangian method to simulate the chip formation in orthogonal cutting and to calculate the temperature distribution within workpiece, chip, and tool. This distribution was used to compute the heat partition between workpiece, chip, and tool in dependence of relevant process parameters. Furthermore, the results were validated by orthogonal cutting experiments and summarized in a formula to calculate the rate of heat flow into the workpiece as a function of those parameters.

Keywords Cutting · Chip formation simulation · Heat partition

✉ Hendrik Puls
h.puls@wzl.rwth-aachen.de

[1] Laboratory for Machine Tools and Production Engineering (WZL), RWTH Aachen University, Steinbachstrasse 19, 52074 Aachen, Germany

1 Introduction

Thermal effects often limit the performance of cutting processes. The energy spent in metal cutting is almost completely converted into heat. Resulting temperature gradients in tool, workpiece, and chip cause heat fluxes and subsequently heating of the tool, workpiece, and machine tool. This often negatively influences the process. On the one hand, a higher heat flux to the tool accelerates tool wear and results in thermal tool and machine tool displacements. On the other hand, a higher heat flux to the workpiece may result in undesired material modifications, burr formation, and also thermal expansion of the work material. Therefore, knowledge about the heat partition is valuable to design the process and coolant system.

In this context, Abukhshim et al. investigated the heat partition in high speed turning of high strength alloy steel to characterize the thermal field in the cutting zone and thus understand the mechanics of high speed machining [1]. For this purpose, they measured cutting forces to determine the total mechanical process power in addition to temperature measurement and finite element analysis. On this basis, they were able to obtain the fraction of heat which flows into the tool and analyzed the influence of the cutting speed.

Sölter and Gulpak studied the heat partition in dry milling with the objective to develop a predictive model for heat induced shape deviations [2]. They also used experimental power and temperature measurement to obtain the ratio β_w of the rate of heat flow into the workpiece $\dot{Q}_w$ to the total mechanical process power P_{mech} by an inverse approach based on finite element analysis. In this case, they

modified a heat flux iteratively until the simulated temperature field agreed with the experimental obtained one. A similar approach to obtain the ratio β_w was used by Joliet et al. who also used a combined experimental and iterative simulation approach [3].

These state of the art methods reveal that the heat partition is commonly calculated by iterative methods. A direct measurement is not possible with state of the art measurement techniques because a very high temporal and spatial temperature resolution would be necessary for this. Furthermore, the temperature field inside the material cannot be measured due to the nature of cutting. Therefore, simulation models are a promising approach. Putz et al. developed a Lagrangian finite element model for a thermomechanical simulation of chip formation to calculate the temperature field in the cutting zone which results from the plastic deformation and friction during the process [4]. From this temperature field, the heat fluxes and heat partition were calculated and analyzed for different tool and process parameters. A similar approach was used by the authors before [5] with the objective to calculate the thermoelastic workpiece deformation in dry cutting. In recent times, the approach was improved by using the coupled Eulerian-Lagrangian finite element method and the analysis was significantly extended, which is presented in this paper.

2 Modeling of chip formation

In this paper, the process of chip formation of orthogonal cutting was simulated by using finite element analysis. The finite element analysis provides a detailed insight into the process physics and allows to calculate the rate of heat flow to workpiece, tool, and chip as well as the calculation of the total required mechanical power.

2.1 Calculation of the heat partition

Before the model design is discussed in detail, the method to determine the rate of heat flow to the workpiece $\dot{Q}_w$ is illustrated in Fig. 1.

For this purpose, the internal heat energy in a moving control volume is evaluated. In the cutting process, a certain heat flux is entering the control volume V_1 inside the workpiece at a certain time t_0. Later, at a time t, the control volume has moved by the distance $l_w = v_c \cdot (t - t_0)$ if the tool is assumed to be fixed. Between t_0 and $t = t_0 + l_w/v_c$, a rate of heat flow $\dot{Q}_w$ has changed the internal heat energy in the volume V_1. If the temperature field reached a steady state, this change of internal heat energy between t_0 and t is the difference of internal heat energy of control volume

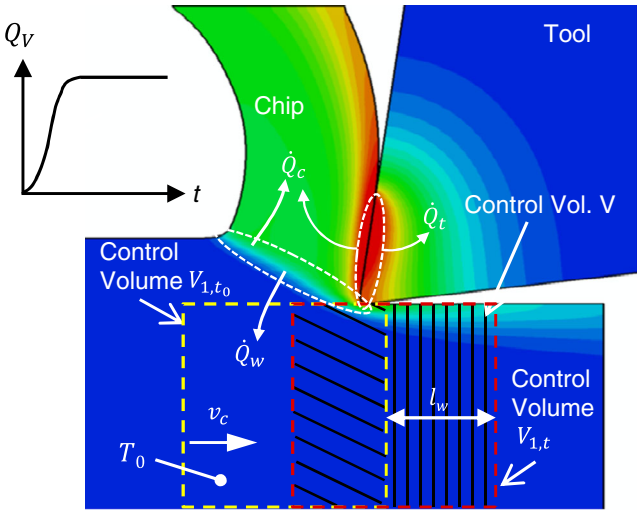

Fig. 1 Control volume method to calculate heat flux into the workpiece

V compared to heat energy inside the volume at temperature T_0:

$$\dot{Q}_w(t) \cong \frac{\Delta Q_w}{t - t_0} = \int_V c_w \cdot \rho_w \cdot (T - T_0) dV \cdot \frac{v_c}{l_w} \tag{1}$$

Furthermore, the internal heat energy inside the tool can be calculated at each timestep by summarizing the internal heat energy of all finite elements of the tool domain to calculate the rate of heat flow into the tool $\dot{Q}_t$.

2.2 Model design and parameters

Figure 2 shows the design of the model which was implemented in the commercial software package ABAQUS Explicit 6-14. Specifically, the coupled Eulerian-Lagrangian technique was used to account for large deformation and material separation in front of the cutting edge.

The basic idea of this method is to simulate the cutting process as a continuous flow of work material against the tool similar to fluid flow. This flow is then separated into workpiece and chip by the tool which acts as an obstacle. The main advantage of this approach is the robust handling of large deformations inside the Eulerian mesh, by using a Lagrangian deformation phase followed by a transport phase. This ensures a continuous remapping of information and variables which can have advantages compared to global remeshing routines, as frequently used within pure Lagrangian models. These methods often try to interpolate data from fine mesh sections to coarser sections which results in loss of information [6]. In addition, the mesh is fixed in space which facilitates the evaluation of state variables at defined locations of the cutting zone. Further

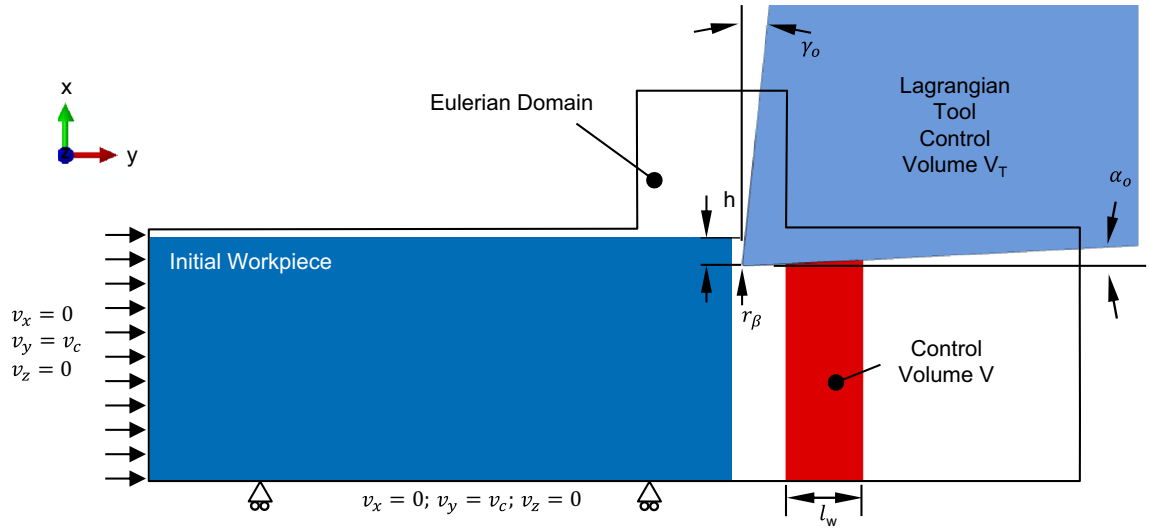

Fig. 2 Coupled Eulerian-Lagrangian model of orthogonal cutting

advantages are the inflow and outflow boundaries. In many cases, the chip and the workpiece far-off the cutting edge are not of interest. Using the CEL method, the work material and the corresponding chip can continuously leave the model domain and thereby reducing the calculation efforts significantly [6].

The model is in fact a 3D model because the CEL method is only implemented for 3D elements in ABAQUS Explicit, but the degree of freedom in z-direction was disabled and the z-thickness of the model comprised only one element. In this model, a minimum element size of 6 µm was used, resulting in approximately 15,000 finite elements. To describe the visco-elastoplastic work material behavior of AISI 1045, a Johnson-Cook model [7] has been utilized using parameters obtained by Klocke et al. [8] (Table 1). The carbide tool was assumed to be rigid and was coated with a (Al,Ti,Cr)-N-Coating (thickness t= 5 µm). The thermal properties for the work material AISI 1045 [9] and tool substrate WC6-Co [10] were taken from literature. Thermal properties for the specific coating were not available. Instead, values for a coating with similar chemical composition AlTiN were used [11]. To model the thermal contact without significant resistance, a heat transfer coefficient of h_t = 10,000 kW/(m^2 K) was utilized. The friction between tool and work material was modeled by a temperature dependent friction model [12]. Below the temperature $T_0 = 450$ °C, a constant friction coefficient of $\mu_0 = 1/\sqrt{3}$ was used. For contact temperatures above T_0, Eq. 2 was used to model a temperature dependent friction coefficient describing thermal softening analog to the Johnson-Cook material model. The model parameters were determined to $m_r = 0.75$ and $T_m = 1500$ °C.

$$\mu = \mu_0 \cdot \left(1 - \left(\frac{T - T_0}{T_m - T_0}\right)^{m_r}\right) \tag{2}$$

Table 1 Johnson-Cook material model for AISI 1045

A (MPa)	B (MPa)	C	n	m	T_m (°C)	ϵ_0 (s^{-1})
546	487	0.027	0.25	0.631	1500	0.001

3 Analysis of heat partition in dry orthogonal cutting of AISI 1045

The model was used to conduct a parameter variation to analyze their quantitative influence on the rate of heat flow into the workpiece and the tool. In addition, the fraction of the rate of heat flow into the workpiece to the total mechanical process power β_w was calculated.

The varied parameters included the most important tool and process parameters in cutting, the uncut chip thickness h, the cutting velocity v_c, the cutting edge radius r_β, the tool orthogonal rake angle γ_o, the flank wear land width VB, the work material temperature T_w, and two different tool coatings.

Figure 3 shows a sample evolution of the chip formation and the computed rate of heat flow into workpiece $\dot{Q}_w$, tool $\dot{Q}_t$, and mechanical process power P_{mech}. After approximately $t \approx 0.3$ ms, the chip starts to leave the Eulerian model domain and after this time, $\dot{Q}_w$ and P_{mech} already almost reached a steady state condition. The heat flux into the tool still decreases significantly due to lower temperature gradients which result from the heating of the tool.

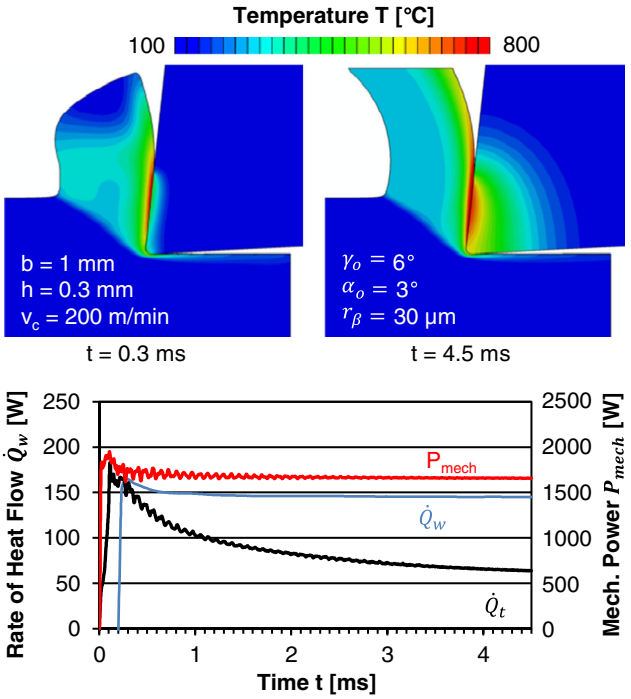

Fig. 3 Sample evolution of the chip formation and the computed rate of heat flow into workpiece $\dot{Q}_w$, tool $\dot{Q}_t$, and mechanical process power P_{mech} in orthogonal cutting of AISI 1045

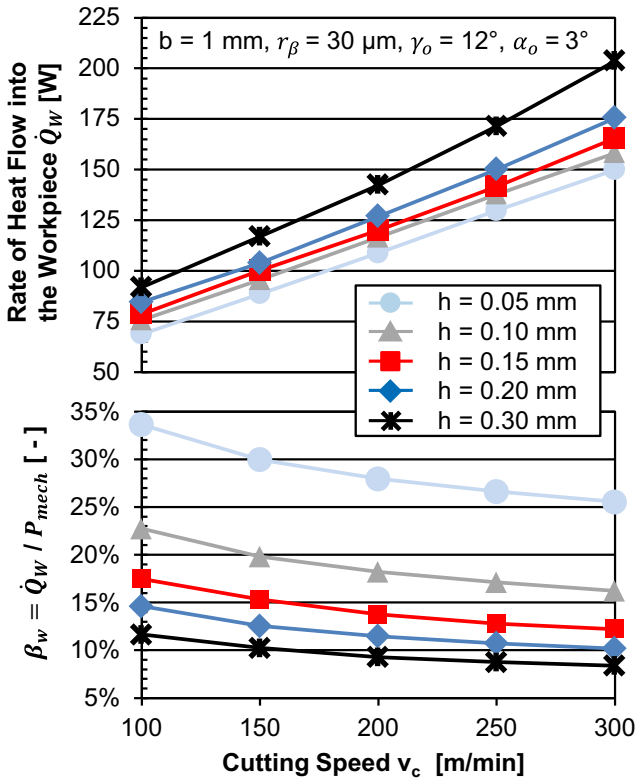

Fig. 4 Effect of uncut chip thickness h and cutting speed v_c on rate of heat flow into workpiece $\dot{Q}_w$ and heat partition β_w

After a cutting time of $t = 4.5$ ms, the thermomechanical energy conversion reached a steady state which represents a cutting length of $l_c = 15$ mm. After this distance all simulations were evaluated.

3.1 Influence of the uncut chip thickness and cutting velocity

Figure 4 shows the effect of uncut chip thickness and cutting velocity on the rate of heat flow into workpiece $\dot{Q}_w$ and the heat partition. It shows an increasing rate of heat flow $\dot{Q}_w$ with rising uncut chip thickness and cutting velocity. However, with an increase of cutting speed by factor 3, $\dot{Q}_w$ only increases by approximately factor 2. This effect is even stronger for an increase of the uncut chip thickness and has several reasons. First, a higher uncut chip thickness and cutting velocity results in a higher fraction of heat which is removed by the chips. The fraction β_w is between 7 and 34 % in the chosen parameter range. The uncut chip thickness increases the distance of the heat to flow from the primary shear zone to the workpiece and the cutting speed reduces the time that is available for this heat transport. Secondly, these technological parameters also modify the process mechanics. An increase in uncut chip thickness and cutting velocity both result in thermal softening in the primary and secondary shear zone which reduces the total heat generation of the process.

In contrast to that, the heat flux into the tool $\dot{Q}_t$ mainly differs with the uncut chip thickness (Fig. 5). The cutting speed only has a minor influence on the heat flux, although the fraction β_w decreases significantly. This means that the heat flux is nearly constant due to a similar temperature gradient and contact zone length but the mechanical process power increases because of the relationship $P_{mech} = F_c \cdot v_c$. The cutting force is slightly decreasing with increasing cutting speed due to thermal softening predominating strain rate hardening.

3.2 Influence of the tool orthogonal rake angle

A variation in the tool orthogonal rake angle results in a highly nonlinear evolution of the rate of heat flow $\dot{Q}_w$ and β_w. With decreasing tool orthogonal rake angle, the plastic deformation of the work material is increased, which can be clearly seen in the temperature rise in Fig. 6. Subsequently, the shear angle ϕ decreases and results in a longer primary shear zone. This provides the generated heat in this shear zone more time to reach the inner work material and to flow into the workpiece. However, an angle over approximately 6° mainly results in a decrease of mechanical process power P_{mech} while the rate of heat flow into the workpiece $\dot{Q}_w$ remains constant (Fig. 7).

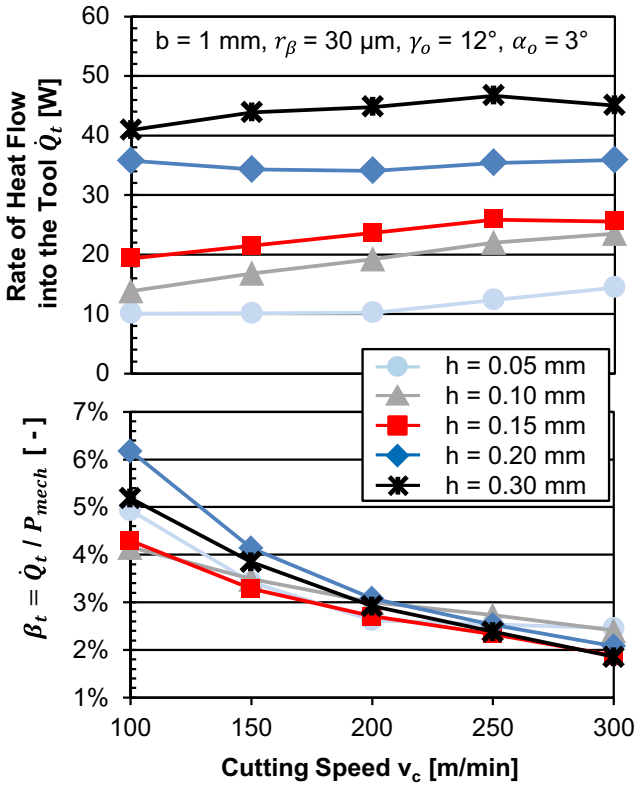

Fig. 5 Effect of uncut chip thickness h and cutting speed v_c on rate of heat flow into tool $\dot{Q}_t$ and heat partition β_w

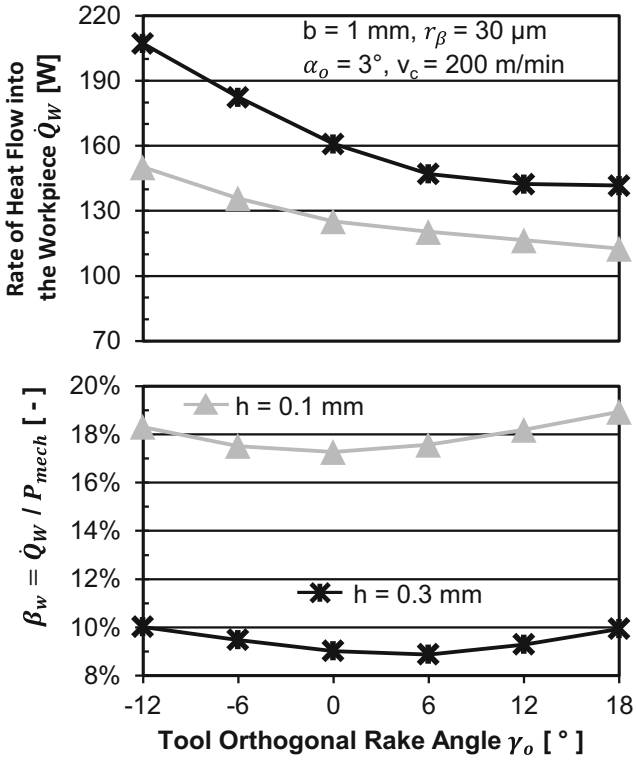

Fig. 7 Effect of tool orthogonal rake angle γ_o on rate of heat flow into workpiece $\dot{Q}_w$ and heat partition β_w

3.3 Influence of the cutting edge radius

The cutting edge radius r_β also has a strong effect on the rate of heat flow into the workpiece but only a minor effect on the mechanical process power P_{mech}. Severe plastic deformation resulting from a larger cutting edge radius generates heat close-by the generated surface. However, it only slightly increases the cutting force and therefore the mechanical process power. Due to the location close to the generated surface, a major fraction of the heat therefore directly flows into the workpiece. The increase of heat generation is also independent on the uncut chip thickness h which is also shown by the constant slope of both curves of the rate of heat flow into the workpiece $\dot{Q}_w$ in Fig. 8.

3.4 Influence of the flank wear land width

The effect described for the cutting edge radius is similar for the flank wear land width VB. The flank wear land width was modeled as a simple plain surface which was inclined by 0.5°, see α_{eff} in Fig. 9. This is necessary in the FE simulation to ensure proper contact, although it might slightly modify the heat generation at the flank face by additional plastic deformation. The cutting edge radius for the worn tool was modeled with a value of $r_\beta = 30$ µm. In reality, the radius is modified by the wear progress, but this was not

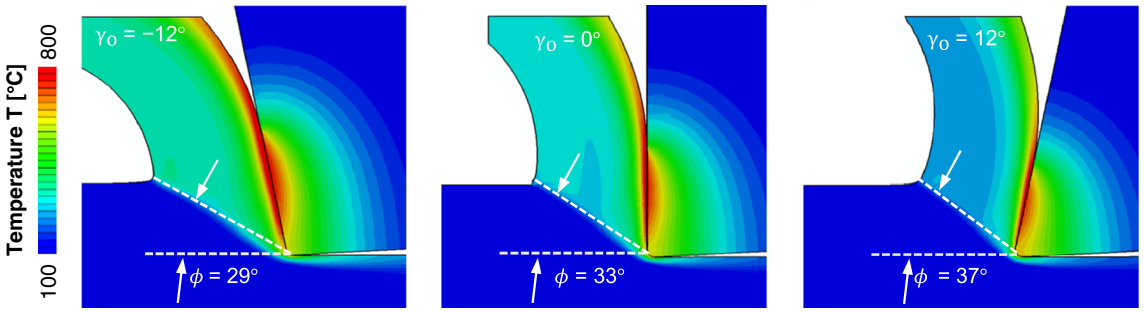

Fig. 6 Effect of tool orthogonal rake angle on shear angle and temperature field

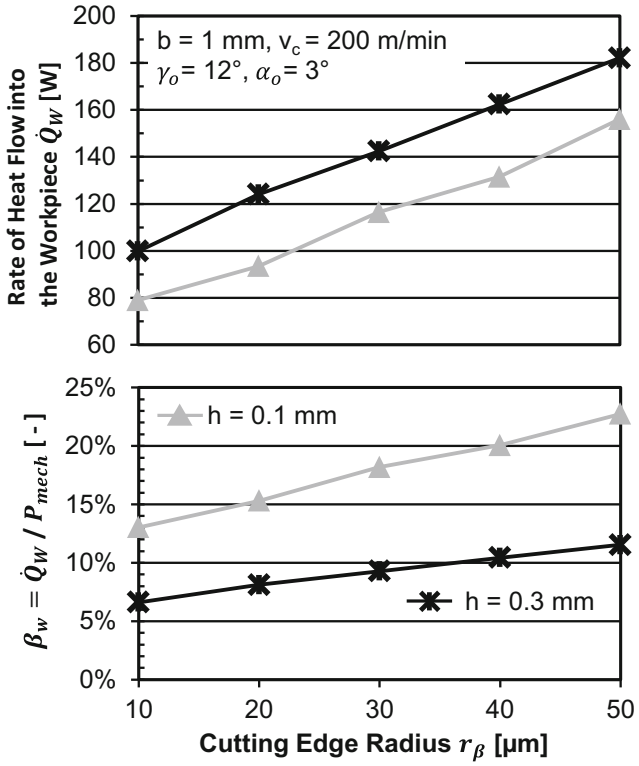

Fig. 8 Effect of cutting edge radius r_β on rate of heat flow into workpiece $\dot{Q}_w$ and heat partition β_w

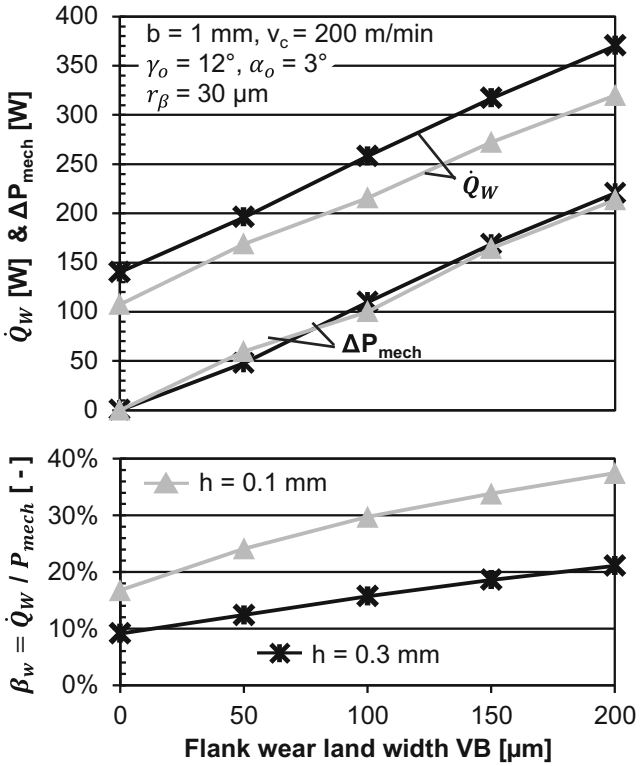

Fig. 10 Effect of flank wear land width VB on rate of heat flow into workpiece $\dot{Q}_w$, rise in mechanical process power ΔP_{mech}, and heat partition β_w

considered in this study as well as crater wear on the rake face.

Flank wear has a strong effect on the rate of heat flow $\dot{Q}_w$ into the workpiece. This was expectable due to the additional contact surface which is generated between work material and worn tool. The frictional power at this interface almost completely flows as heat into the workpiece which is shown by the slope of ΔP_{mech} in Fig. 10. Analogously to the cutting edge radius r_β, the increase of the rate of heat flow into the workpiece $\dot{Q}_w$ is independent from the uncut chip thickness h.

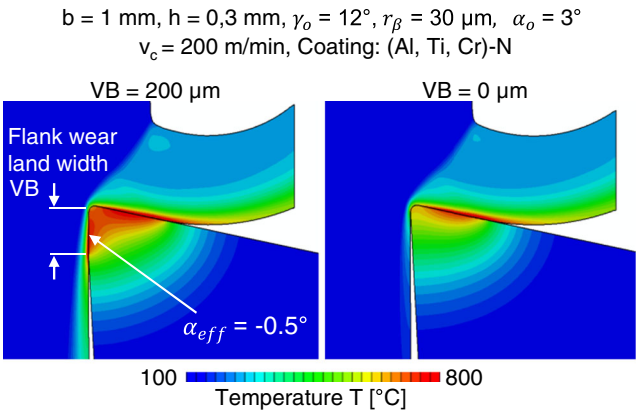

Fig. 9 Comparison of two sample temperature fields for different wear states

3.5 Influence of the work material temperature

After the analysis of the influence of basic tool and process parameters in Sections 3.1–3.4, it is also relevant to analyze the work material temperature T_w. In dry cutting processes, the material is continuously heated by the process itself. This temperature rise results in softening of the material and also differences in the temperature gradients in the cutting zone. Therefore, the total energy conversion as well as the partition of the generated heat might be different. Figure 11 shows the influence of the work material temperature T_w on the rate of heat flow into the workpiece $\dot{Q}_w$. The heat flow is decreasing by 12–16 % for the chosen parameters for a temperature increase from 30 to 200 °C. The fraction β_w remains almost constant which means that the temperature gradients and heat partition do not change significantly.

3.6 Influence of the tool coating

The last investigated parameter was the coating of the tool. For this purpose, the rate of heat flow into workpiece and

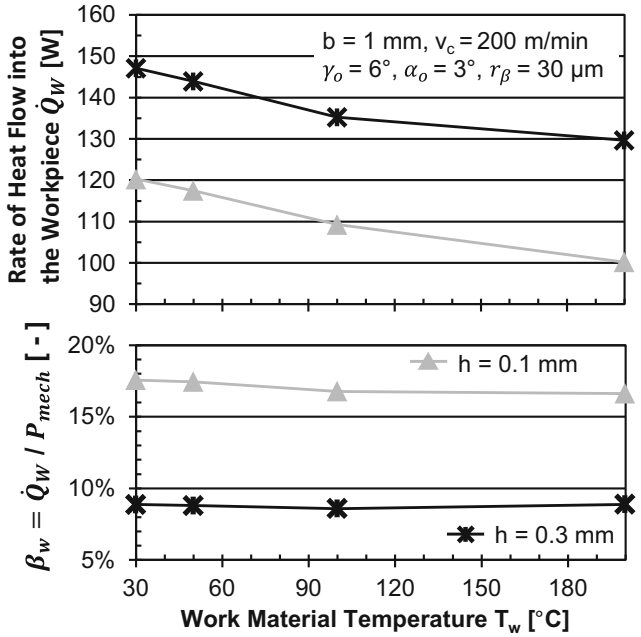

Fig. 11 Effect of the work material temperature T_w on the rate of heat flow into the workpiece $\dot{Q}_w$ and heat partition β_w

tool was calculated for a AlTiN and a TiN coating. The thermal properties were taken from literature [11]. The thermal conductivity of the TiN was modeled approximately five times higher compared to AlTiN. However, there is only a small difference of the rate of heat flow into the workpiece. The modified temperature gradient in the tool due to the different thermal properties only results in increased heat flow (+14 and +18 % for the TiN compared to AlTiN coating) into the tool (Fig. 12).

3.7 Model validation

To validate the model, an orthogonal cutting process was realized on a vertical broaching machine tool to measure the cutting force components for selected simulated parameters. The machine tool has two linear position axes and a

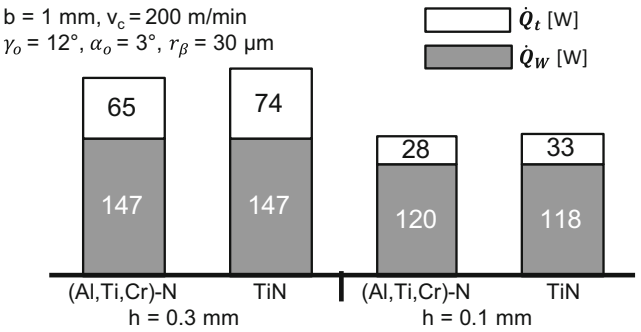

Fig. 12 Effect of the coating on the rate of heat flow into the workpiece $\dot{Q}_w$ and tool $\dot{Q}_t$

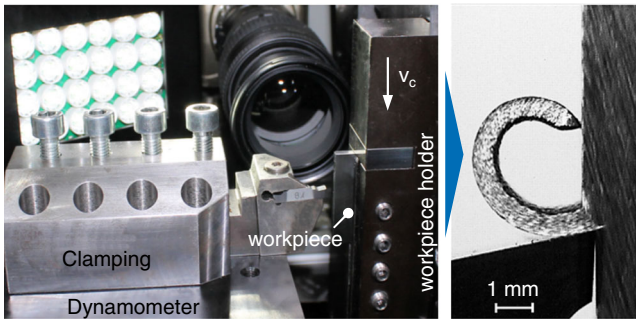

Fig. 13 Orthogonal cutting in external broaching machine tool

third linear axis to conduct the cutting movement. The linear drive that usually carries the broaching tool provides a maximum cutting speed of 150 m/min at a maximum cutting force of 80 kN. In this case, a workpiece holder is mounted on the linear drive and the tool is fixed on a dynamometer, Fig. 13. Figure 14 shows the comparison between simulated and measured cutting force components. Especially the cutting force F_c (y-direction, see Fig. 2) shows a very good agreement. This force component defines the total mechanical process power and is therefore the most important indicator for the model validation. The deviation between simulated and measured feed force F_f (x-direction, see Fig. 2) is for some cases higher than for the cutting force. It is assumed that the real cutting edge has no ideal radius as assumed in the simulation model and there is also a uncertainty when measuring the cutting edge radius. Furthermore, additional deviations due to the model assumptions and submodels are inevitable. An additional thermal validation of the model can be found in [5] and [12].

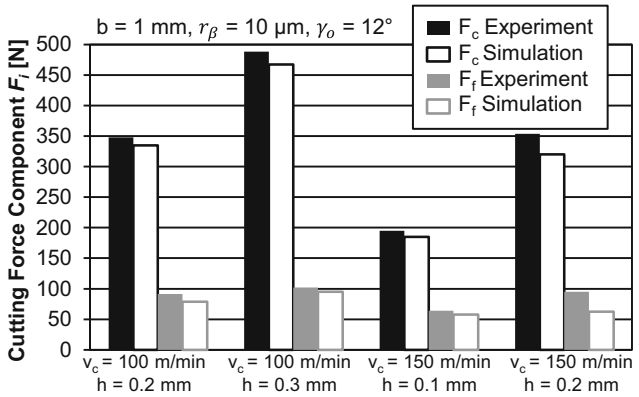

Fig. 14 Comparison between simulated and measured cutting force components

4 Mathematical model to calculate the rate of heat flow into the workpiece

The simulation results were summarized in a mathematical model according to Eq. 3 in order to calculate the rate of heat flow into the workpiece for any combination of the width of cut b, the uncut chip thickness h, the tool orthogonal rake angle γ_o, cutting edge radius r_β, flank wear land width VB, and cutting speed v_c for the specific work material AISI 1045. The coating was not considered because the simulation results in Fig. 12 indicate a weak influence of the coating on the rate of heat flow into the workpiece.

$$\dot{Q}_w = f(b, h, \gamma_o, r_\beta, VB, v_c, T_w; K_1, ..., K_n) \tag{3}$$

To obtain parameters $K_1 ... K_n$, a nonlinear regression analysis was conducted according to Eq. 4. The variable number m represents the number of simulations which were conducted and analyzed in Section 3.

$$\sum_{i=0}^{m} (f(b, h, \gamma_o, r_\beta, VB, v_c, T_w; K_1, ..., K_n) - \dot{Q}_{w,i})^2 = min \tag{4}$$

To solve this problem, a model function was developed based on the relationships that were analyzed in Section 3. First of all, Eq. 1 was modified to Eq. 5. This equation assumes that the amount of heat in a control volume is proportional to the width of cut b since there is no large temperature gradient perpendicular to feed and cutting speed vector for a two-dimensional process. In addition, the length of the control volume was replaced by factor K_s. Now, the relationship between ΔQ_w and uncut chip thickness h, cutting speed v_c, cutting edge radius r_β, orthogonal rake angle γ_o, work material temperature T_w, and flank wear land width VB has to be established.

$$\dot{Q}_w = K_s \cdot \Delta Q_w \cdot v_c \cdot b \tag{5}$$

For this reason, the individual variables were evaluated and individual terms were created. First of all, a basic term $(K_s + K_h \cdot h)$ was created which represents the heat flow from the primary shear zone into the workpiece. It is concluded that this heat increases proportional to the uncut chip thickness h, Fig. 4. In addition, the projected length of the primary shear zone $l_s = h \ */ \tan(\phi)$ in cutting speed direction can be modified by changing the orthogonal rake angle. As it can be seen in Fig. 6, the shear angle can be reduced by a decreasing rake angle. In this case, the projected length of the shear zone l_s increases, so the heat has more time to flow from the primary shear zone to the inner workpiece. To include this influence in the function, the basic term was multiplied with a nonlinear term $(1 + K_{\gamma 1}(\gamma_o + 30)^{K_{\gamma 2}})$. A number of 30 was added to the rake angle to avoid negative numbers.

To include the influence of the cutting edge radius r_β, a linear term $K_r(30 - r_\beta)$ was added to the basic term because the heat generation at the cutting edge is assumed to be independent on the uncut chip thickness and rake angle. A value of 30 µm was chosen as a reference value.

The same assumption was made for the flank wear land width K_{VB}. The heat generation at the flank face mainly depends on the friction stress, cutting speed, and the area of the flank wear land.

To account for the thermal softening, the terms which describe the heat flow from the primary shear zone, deformation at the cutting edge and friction at the flank wear were multiplied by two terms because the thermal softening reduces the heat generation for all three mechanism. First, a linear term $\left[1 + K_{T_w}(30 - T_w)\right]$ describes the thermal softening by work material heating. A second term $v_c^{K_v}$ defines the relationship between thermal softening and cutting speed.

Finally, the equation can be summarized as follows. This equation was used to solve the nonlinear regression (4) by the Levenberg-Marquardt algorithm. The calculated parameters and variable units can be found in Table 2. The range of validity was not validated explicitly but it is assumed that the equation is valid for conventional conditions which were used in the simulations: 100 m/min $\leq v_c \leq$ 300 m/min, 0.05 mm $\leq h \leq$ 0.3 mm, 10 µm $\leq r_\beta \leq$ 50 µm, $-12° \leq \gamma_o \leq 18°$, 0 µm $\leq$ VB $\leq$ 200 µm and 30 °C $\leq T_w \leq$ 200 °C. The maximum deviation between simulation result and mathematical model was 8.4 % for the evaluated simulations. The coefficient of determination was $R^2 = 0.994$.

$$\begin{aligned}\dot{Q}_w = &\left[(K_s + K_h \cdot h)(1 + K_{\gamma 1}(\gamma_o + 30)^{K_{\gamma 2}}) + K_r(30 - r_\beta)\right. \\ &\left. + K_{VB} \cdot VB\right] \cdot \left[1 + K_{T_w}(30 - T_w)\right] \cdot v_c^{K_v} \cdot b\end{aligned} \tag{6}$$

This equation serves to calculate the rate of heat flow into the workpiece as a function of all relevant parameters for the normalized work material AISI 1045 in orthogonal cutting. Furthermore, it could be used to estimate the rate of heat flow for nearly all cutting operations of AISI 1045, if

Table 2 Model parameters and variable units

Parameter	Value	Variable	Unit
K_h	317.398	$\dot{Q}_w$	(W)
K_s	206.648	h	(mm)
K_{VB}	0.02311	VB	(µm)
K_{T_w}	0.00111	T_w	(°C)
K_r	−0.04176	r_β	(µm)
K_v	0.72785	v_c	(m/min)
$K_{\gamma 1}$	−0.97460	γ_o	(°)
$K_{\gamma 2}$	0.00414		

the chip cross sectional area is divided into discrete sections along the cutting edge and if other possible changes in the boundary conditions are considered.

5 Conclusions

In this paper, a method to analyze the heat partition in dry metal cutting was presented. The method is based on a coupled Eulerian-Lagrangian finite element method and calculates the thermomechanical energy conversion of the continuous chip formation process. The resulting temperature fields in workpiece, chip, and tool were evaluated to calculate the rate of heat flow into the workpiece and tool. In addition, the total mechanical process power was calculated and compared to the rates of heat flow. The analysis has shown that the heat flow into the workpiece is significantly influenced by nearly all cutting and tool parameters. Following conclusions could be drawn:

1. For the same machined volume, the heat input into the workpiece $\dot{Q}_w$ is lower for higher material removal rates due to the shortened process time. Furthermore, higher uncut chip thickness h (feed) or cutting speed v_c will remove more heat with the chip.
2. The tool orthogonal rake angle γ_o has a nonlinear influence on the rate of heat flow into the workpiece. It decreases significantly by changing the rake angle from negative to positive due to less plastic deformation and higher shear angles.
3. The cutting edge radius r_β and flank wear land width VB have both a linear major influence on the rate of heat flow into the workpiece. A large radius or significant flank wear doubles or even triples the rate of heat flow into the workpiece compared to a sharp or new tool. However, in this study, crater wear and a modification of the cutting edge by wear were not considered.
4. Due to the nature of cutting, the machined work material is mostly preheated by prior cutting. The effect of the preheated work material temperature is less significant compared to the other parameters and effects but however should be considered.
5. Different thermophysical properties of tool coatings do not significantly modify the rate of heat flow into the workpiece but influence the rate of heat flow to the tool.
6. Within the simulation range of cutting and tool parameters, the fraction $\beta_w = \dot{Q}_w / P_{mech}$ was between 6.6 and 37.8 %. This fraction strongly depends on the cutting parameters and tool geometry. Therefore, the estimation of the rate of heat flow $\dot{Q}_w$ by using a constant β_w and calculating the mechanical power P_{mech} is not reasonable.
7. The findings have been summarized in Eq. 6 which can be used to calculate the rate of heat flow into the workpiece as a function of all relevant parameters for the specific work material AISI 1045. Although it was obtained in orthogonal cutting, it can be used to estimate the rate of heat flow for milling, turning, and broaching operations. This in turn can be utilized in advanced simulation models to compensate thermal effects of the cutting process. A reasonable approach for this purpose would be the discretization of the chip cross sectional area along the cutting edge and the consideration of the material preheating by previous cutting teeth (milling and broaching) or workpiece revolutions (turning) in the simulation model.

Acknowledgments The authors would like to thank the German Research Foundation (DFG) for the funding of the depicted research within the priority programme 1480, GZ KL500/79-2 and GZ KL500/79-3.

References

1. Abukhshim NA, Mativenga PT, Sheikh MA (2005) Investigation of heat partition in high speed turning of high strength alloy steel. Int J Mach Tools Manuf 45(15):1687–1695
2. Sölter J, Gulpak M (2012) Heat partitioning in dry milling of steel. CIRP Ann Manuf Technol 61:87–90
3. Joliet R, Byfut A, Kersting P, Schrder A, Zabel A (2013) Validation of a heat input model for the prediction of thermomechanical deformations during NC milling. Procedia CIRP 8:402–407
4. Putz M, Schmidt G, Semmler U, Dix M, Brunig M, Brockmann M, Gierlings S (2015) Heat flux in cutting: importance, simulation and validation. Procedia CIRP 31:333–339
5. Klocke F, Lung D, Puls H (2013) FEM-Modelling of the thermal workpiece deformation in dry turning. Procedia CIRP 8:240–245
6. Klocke F, Lung D, Puls H (2014) Coupled Eulerian-Lagrangian modelling of high speed metal cutting processes. In: Kolr P (ed) 11th international conference on high speed machining. Czech Machine Tool Society, Czech Republic
7. Johnson GR, Cook WH (1983) A constitutive model and data for metals subjected to large strains, high strain rates and high temperatures. In: Proceedings of the 7th int. symposium on ballistics, pp 541–547
8. Klocke F, Lung D, Buchkremer S (2013) Inverse identification of the constitutive equation of inconel 718 and AISI 1045 from FE machining simulations. Procedia CIRP 8:212–217
9. Spittel M, Spittel T (2009) Steel symbol/number: C45/1.0503. In: Warlimont H (ed) Springer materials - the Landolt-Brnstein database. Springer, Berlin/Heidelberg
10. Beiss P, Ruthhardt R, Warlimont H (2002) Powder metallurgy data. refractory, hard and intermetallic materials, Landolt-Brnstein - Group VIII advanced materials and technologies. Springer, Berlin/Heidelberg
11. Martan J, Bene P (2012) Thermal properties of cutting tool coatings at high temperatures. Thermo-chemica Acta 539:51–55
12. Puls H (2015) Mehrskalenmodellierung thermo-elastischer Werkstckdeformationen beim Trockendrehen, Dissertation, RWTH Aachen University